Run	Event	Ctrk(Sump)	Ctrk(N)	Ecal(SumE)	Hcal(SumE)	event display based classification	cut based classification
4353	5960	65.3	45	51.3	2.4	$Z^0 \rightarrow$ hadrons	$Z^0 \rightarrow$ hadrons
4353	6317	25.6	44	47.3	5.2	$Z^0 \rightarrow$ hadrons	$Z^0 \rightarrow$ hadrons
4353	7137	97.0	2	2.2	8.9	$Z^0 \rightarrow \mu^+\mu^-$	$Z^0 \rightarrow \mu^+\mu$
4353	7635	24.6	33	43.4	14.8	$Z^0 \rightarrow$ hadrons	$Z^0 \rightarrow$ hadrons
4353	9149	95.2	2	1.3	7.9	$Z^0 \rightarrow \mu^+\mu^-$	$Z^0 \rightarrow \mu^+\mu^-$
4353	9289	22.7	2	34.4	0	$Z^0 \rightarrow e^+e^-$	$Z^0 \rightarrow \tau^+\tau^-$
4353	9422	43.8	28	61.8	12.1	$Z^0 \rightarrow$ hadrons	$Z^0 \rightarrow$ hadrons
4353	9595	54.7	26	72.4	1.2	$Z^0 \rightarrow$ hadrons	$Z^0 \rightarrow$ hadrons
4353	12071	1.6	4	2.3	0	$Z^0 \rightarrow \tau^+\tau^-$	$Z^0 \rightarrow \tau^+\tau^-$
4353	20330	78.2	2	90.5	0	$Z^0 \rightarrow e^+e^-$	$Z^0 \rightarrow e^+e^-$
4353	21251	106.2	2	2.6	3.6	$Z^0 \rightarrow \mu^+\mu^-$	$Z^0 \rightarrow \mu^+\mu^-$
4353	22997	90.5	2	93.2	0	$Z^0 \rightarrow e^+e^-$	$Z^0 \rightarrow e^+e^-$
4353	23669	35.4	6	16.0	20.1	$Z^0 \rightarrow \tau^+\tau^-$	$Z^0 \rightarrow \tau^+\tau^-$
4353	24086	90.7	2	92.9	0.6	$Z^0 \rightarrow e^+e^-$	$Z^0 \rightarrow e^+e^-$
4353	24128	93.8	2	1.9	9.4	$Z^0 \rightarrow \mu^+\mu$	$Z^0 \rightarrow \mu^+\mu$
4353	27237	29.1	2	21.6	3.8	$Z^0 \rightarrow \tau^+\tau^-$	$Z^0 \rightarrow \tau^+\tau$
4353	27314	93.1	4	92.9	0	$Z^0 \rightarrow e^+e^-$	$Z^0 \rightarrow e^+e$
4353	28367	97.5	2	2.5	3.6	$Z^0 \rightarrow \mu^+\mu$	$Z^0 \rightarrow \mu^+\mu$
4353	30444	3.9	2	4.2	0	$Z^0 \rightarrow \tau^+\tau$	$Z^0 \rightarrow \tau^+\tau$
4353	33656	69.4	2	92.9	0.2	$Z^0 \rightarrow e^+e$	$Z^0 \rightarrow e^+e$

Table 4: Measured values and classification results for the sample TEST2

5. Part II: Statistical analysis of Z^0 decays

This part is dedicated to the analysis of large data samples. This is required for an appropriate precision in the measurement of the Z^0 parameters (e.g. Z^0 mass and decay width). An analysis based on event displays is hence no longer feasible. The software PAW is used for the statistical analysis, which works with samples called *ntuples*. PAW allows the user to set cuts on certain variables and apply them to the *ntuple*. Finally the resulting distributions for each variable can be plotted as a histogram. The variables available to us are the same as in section 4 with some additions and renamings[1]:

- NCHARGED: Number of charged tracks (previously Ctrk(N))
- PCHARGED: Total scalar sum of track momenta in GeV (previously Ctrk(Sump))
- E_ECAL: Total energy deposited in the electromagnetic calorimeter in GeV (previously Ecal(SumE))
- E_HCAL: Total energy deposited in the hadronic calorimeter in GeV (previously Hcal(SumE))
- E_LEP: Energy of the LEP beam in GeV ($\sqrt{s}/2$)
- COS_THRU: Cosine of the angle between beam axis and thrust axis
- COS_THET: Cosine of the angle between incoming positron and outgoing positive particle

5.1. Determination of cuts for particle identification

Similar to Part I (section 4), there are four sets of Monte Carlo generated samples available. One for each of the four decay modes described in section 4. Additionally there is one out of six possible data samples with unknown decay channels. The second data sample was assigned to us for this part of the analysis.

The cuts are also determined in a similar fashion to section 4.1. Histograms for each of the variables are plotted and examined. Once a discriminating variable is found, it is plotted in a restricted interval to improve the accuracy of the cut. This process is repeated until each decay channel can be identified. Due to the increase in statistics compared to the analysis in section 4.1, it is possible to refine the cuts from this section using the process described above.

As an example of how this process starts, the distribution of all variables for the Monte Carlo and data samples is shown in Figures 15, 16, 17, 18 and 19 in the appendix. The variable E_LEP is not plotted for the Monte Carlo generated samples, because they were all simulated at the same energy of 91.22 GeV. The figures show, that some distributions are nonsensical (e.g. peak for COS_THET at 1000 for the electron sample). These are standard values in case of an erroneous measurement and can be filtered with appropriate cuts.

Before any particle identification is done, a set of cuts is applied. Namely $0 <$ PCHARGED < 130 and NCHARGED > 0. The first cut is done, because events with PCHARGED ≤ 0 would be unphysical and events with PCHARGED ≥ 130 would clearly exceed LEP's energy. The second cut is done, because all decay channels we are interested in require at least one charged track in the detector. Regardless of any other cuts for particle identification, this set of cuts will always be applied and referred to as pre-selection cuts. The distributions of variables for each of the four Monte Carlo samples with pre-selection cuts applied can be found in Figures 20, 21, 22 and 23 in the appendix.

The final cuts used for particle identification are shown in Figure 13 in a tree-like diagram. The cut after the classification as $Z^0 \rightarrow e^+e^-$ event is needed to isolate the s-channel. This can be done due to the angular dependence of s- and t-channel on θ (see section 2.2). Likewise, the cut after the classification as $Z^0 \rightarrow \mu^+\mu^-$ is needed to remove unphysical events. This is especially important, because the variable COS_THET will be needed to measure the forward backward asymmetry.

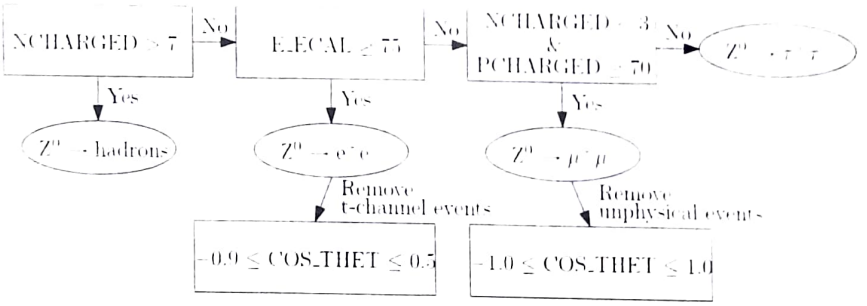

Figure 13: The cuts used to differentiate between different decay channels of the Z^0 boson for Part II. The diagram has to be interpreted in such a way, that each node of the tree contains all cuts of previous nodes.

5.2. Efficiency matrix

The determined cuts can now be used on the Monte Carlo generated events. By observing how the samples for each decay mode are classified, it is possible to obtain an efficiency matrix ϵ_{mat}. It is a measure for the effectiveness of our cuts. In an ideal case it is diagonal. An efficiency matrix can be defined in the following way.

Let N_{obs} be the vector with the observed number of events for each decay channel, N_{phys} be the vector with the actual physical number of events for each decay channel and ϵ_{mat} be the efficiency matrix. Then

$$N_{obs} = \epsilon_{mat} N_{phys} \qquad \Leftrightarrow \qquad N_{phys} = \epsilon_{mat}^{-1} N_{obs}. \tag{7}$$

The matrix can be obtained from the values given in Table 5. It shows the resulting number of events classified to belong to the respective decay channel after applying the cuts from section 5.1.

Monte Carlo sample	number of events classified as				number of
	$Z^0 \to e^+e^-$	$Z^0 \to \mu^+\mu^-$	$Z^0 \to \tau^+\tau^-$	$Z^0 \to$ hadrons	events in sample
electron sample	20688	631	679	6	51657
muon sample	1	82685	4569	0	89334
tauon sample	116	495	77116	539	78621
hadron sample	0	0	963	96659	97669

Table 5: Number of events classified to belong to the respective decay channel after the cuts from section 5.1 have been applied to the Monte Carlo samples.

It should be noted, that the number of electrons from the electron Monte Carlo sample is too low, because of the cut to isolate the s-channel contribution. Hence, using the s-channel distribution $(1 + \cos^2\theta)$, their number has to be corrected by the factor given in equation 8. This gives a corrected value of 32747, instead of 20688.

$$\frac{\int_{-1}^{1} 1 + \cos^2\theta \, d\cos\theta}{\int_{-0.9}^{0.5} 1 + \cos^2\theta \, d\cos\theta} \approx 1.5829 \tag{8}$$

The efficiency matrix ϵ_{mat} can now be obtained by dividing the number of classified events by the total number of events in the respective sample. Applying this step to every line in Table 5 gives:

$$\epsilon_{mat} = \begin{pmatrix} 6.34 \times 10^{-1} & 1.22 \times 10^{-2} & 1.31 \times 10^{-2} & 1.16 \times 10^{-4} \\ 1.12 \times 10^{-5} & 9.26 \times 10^{-1} & 5.11 \times 10^{-2} & 0.00 \\ 1.48 \times 10^{-3} & 6.30 \times 10^{-3} & 9.81 \times 10^{-1} & 6.86 \times 10^{-3} \\ 0.00 & 0.00 & 9.86 \times 10^{-3} & 9.90 \times 10^{-1} \end{pmatrix}^T$$

$$= \begin{pmatrix} 6.34 \times 10^{-1} & 1.12 \times 10^{-5} & 1.48 \times 10^{-3} & 0.00 \\ 1.22 \times 10^{-2} & 9.26 \times 10^{-1} & 6.30 \times 10^{-3} & 0.00 \\ 1.31 \times 10^{-2} & 5.11 \times 10^{-2} & 9.81 \times 10^{-1} & 9.86 \times 10^{-3} \\ 1.16 \times 10^{-4} & 0.00 & 6.86 \times 10^{-3} & 9.90 \times 10^{-1} \end{pmatrix}$$

Transposing is required in order to be consistent with the relations from equation 7, because they apply to column vectors. Next the errors need to be calculated. Whether or not an event passes a series of cuts can be seen as a random experiment with two outcomes. The error can thus be estimated by the standard deviation of a binomial distribution[1]

$$\Delta\epsilon = \sqrt{\frac{\epsilon}{N} \cdot (1 - \epsilon)}$$

, where ϵ refers to a single element from ϵ_{mat} and N to the respective number of total events given in Table

[1] This method was explained to us beforehand, but can also be found in Prof. Dingfelders lecture on *Statistical Methods of Data Analysis* from the summer term 2018.

E_{CMS} / GeV	88.47	89.46	90.22	91.22	91.97	92.96	93.71
N_{obs}							
N_e	73	189	229	1747	327	110	89
N_μ	77	197	276	2493	564	194	148
N_τ	135	289	355	3184	675	287	182
N_{had}	1993	4826	6845	61 089	12 911	5105	3447
N_{phys}							
N_e	115 ± 13	298 ± 22	361 ± 24	2750 ± 67	515 ± 29	173 ± 17	140 ± 15
N_μ	81 ± 9	207 ± 15	292 ± 18	2641 ± 54	599 ± 26	206 ± 15	157 ± 13
N_τ	112 ± 12	231 ± 17	272 ± 19	2451 ± 61	519 ± 27	228 ± 17	140 ± 14
N_{had}	2013 ± 45	4875 ± 70	6915 ± 84	61 710 ± 251	13 042 ± 115	5157 ± 72	3482 ± 59

Table 6: Number of recorded events with applied cuts and the number of events corrected by the efficiency matrix.

E_{CMS} / GeV	88.47	89.46	90.22	91.22	91.97	92.96	93.71
σ_e / pb	0.40 ± 0.04	0.81 ± 0.05	1.31 ± 0.06	1.85 ± 0.03	1.17 ± 0.05	0.49 ± 0.05	0.32 ± 0.04
σ_μ / pb	0.31 ± 0.03	0.62 ± 0.03	1.13 ± 0.05	1.79 ± 0.03	1.33 ± 0.05	0.58 ± 0.04	0.36 ± 0.04
σ_τ / pb	0.39 ± 0.03	0.67 ± 0.04	1.08 ± 0.05	1.70 ± 0.03	1.18 ± 0.05	0.64 ± 0.05	0.32 ± 0.04
σ_{had} / pb	7.41 ± 0.13	14.28 ± 0.17	25.97 ± 0.28	40.57 ± 0.25	28.82 ± 0.30	14.56 ± 0.26	8.25 ± 0.20

Table 7: Calculated cross sections for all decay channels with equation 9 for different center of mass energies. The error was calculated by Gaussian error propagation.

5.3.2. Forward-backward asymmetry

Weinberg angle

The forward-backward asymmetry of the muon final states can be investigated by considering the events in forward and backward direction. In our set, this can be done by analyzing the number of events $N_{\text{Forward, Backward}}$ for $\cos\theta > (<)0$.
The forward-backward asymmetry is given by equation 2:

$$A_{FB} = \frac{\int_0^1 \frac{d\sigma}{d\cos\theta} d\cos\theta - \int_{-1}^0 \frac{d\sigma}{d\cos\theta} d\cos\theta}{\int_0^1 \frac{d\sigma}{d\cos\theta} d\cos\theta + \int_{-1}^0 \frac{d\sigma}{d\cos\theta} d\cos\theta} = \frac{\sigma_F - \sigma_B}{\sigma_F + \sigma_B} + C_{AS} = \frac{N_F - N_B}{N_F + N_B} + C_{AS}$$

The radiation corrections C_{AS} are given in [1]. The resulting values are listed in Table 8.
With the forward-backward asymmetry it is now possible to calculate the Weinberg angle $\sin^2\theta_W$. Near the Z^0 resonance it is given by equation 3 The closest value to M_Z is 90.22 GeV, so the Weinberg angle is determined with this value (see table 8). Since the Monte Carlo sample is also simulated at this energy. $\sin^2\theta_W$ was also calculated for this sample (table 8).
The results agree with the literature value of $\sin\theta_W = 0.2312$ [1] within one standard deviation.

5. Using this, the following uncertainties are obtained:

$$\Delta\epsilon_{\text{mat}} = \begin{pmatrix} 2.12 \times 10^{-3} & 1.12 \times 10^{-5} & 1.37 \times 10^{-4} & 0.00 \\ 4.83 \times 10^{-4} & 8.78 \times 10^{-4} & 2.82 \times 10^{-4} & 0.00 \\ 5.01 \times 10^{-4} & 7.37 \times 10^{-4} & 4.89 \times 10^{-4} & 3.16 \times 10^{-4} \\ 4.74 \times 10^{-5} & 0.00 & 2.94 \times 10^{-4} & 3.24 \times 10^{-4} \end{pmatrix}.$$

Though for calculations on the data sample, the inverse of the efficiency matrix is needed. An explanation for this can be found in equation 7. The vector N_{phys} is not known for the data sample and thus has to be determined from the inverted efficiency matrix and N_{obs}, which is obtained by using the cuts from section 5.1 on the data sample. The Python programming language provides a numerical matrix inversion algorithm within the package numpy. Hence this algorithm is used for any matrix inversion in this report. However the calculation of $\Delta\epsilon_{\text{mat}}^{-1}$ is not as trivial. It is given in [10] to be:

$$(\Delta\epsilon_{\text{mat}}^{-1})^2_{\alpha\beta} = (\epsilon_{\text{mat}}^{-1})^2_{\alpha\delta}(\Delta\epsilon_{\text{mat}})^2_{\delta\gamma}(\epsilon_{\text{mat}}^{-1})^2_{\gamma\beta}$$

Hence the following matrices are obtained:

$$\epsilon_{\text{mat}}^{-1} = \begin{pmatrix} 1.58 & 1.12 \times 10^{-4} & -2.37 \times 10^{-3} & 2.36 \times 10^{-5} \\ -2.07 \times 10^{-2} & 1.08 & -6.91 \times 10^{-3} & 6.88 \times 10^{-5} \\ -2.01 \times 10^{-2} & -5.64 \times 10^{-2} & 1.02 & -1.02 \times 10^{-2} \\ -4.62 \times 10^{-5} & 3.90 \times 10^{-4} & -7.07 \times 10^{-3} & 1.01 \end{pmatrix}$$

$$\Delta\epsilon_{\text{mat}}^{-1} = \begin{pmatrix} 5.27 \times 10^{-3} & 2.27 \times 10^{-5} & 2.20 \times 10^{-4} & 2.32 \times 10^{-6} \\ 8.27 \times 10^{-4} & 1.03 \times 10^{-3} & 3.11 \times 10^{-4} & 3.80 \times 10^{-6} \\ 8.10 \times 10^{-4} & 8.15 \times 10^{-4} & 5.09 \times 10^{-4} & 3.26 \times 10^{-4} \\ 7.60 \times 10^{-5} & 1.77 \times 10^{-5} & 3.03 \times 10^{-4} & 3.31 \times 10^{-4} \end{pmatrix}$$

5.3. Analysis of OPAL data

5.3.1. Event numbers and cross section

With the done preparatory work it is now possible to analyse a data set of real OPAL data. We got the set daten2. The events were recorded on different energies. In Figure 19 in the appendix the distribution of the different variables can be seen.
First, we want to know the number of events N_{obs} in the different decay channels. To separate the center of mass energies we first choose energy intervals. Surprisingly there are not only the discrete energies given in [1], but contributions of many different energies. With the chosen intervals all different energies are included.

To analyze the data, the cuts for the different channels (see fig. 13) were applied. The received number of events can be seen in table 6. To obtain the real number N_{phys} one has to correct the values with the efficiency matrix, which was calculated in section 5.2. The results can also be found in table 6. The error is calculated with Gaussian error propagation, where $\Delta N_{\text{obs}} = \sqrt{N_{\text{obs}}}$.
To calculate the cross sections in the hadronic and leptonic decay channels the relation

$$\sigma = \frac{N_{\text{phys}}}{\int \mathcal{L}\,\mathrm{d}t} + C(E_{\text{CMS}}) \tag{9}$$

is used. The integrated luminosity $\int \mathcal{L}\,\mathrm{d}t$, its error and the radiation correction factor $C(E_{\text{CMS}})$ are known from [1] and [11]. With these values it is possible to determine the cross section. For the results, see Table 7.

E_{CMS}/GeV	88.47	89.46	90.22	91.22	91.97	92.96	93.71	Monte Carlo
N_f	40	91	156	1219	281	68	70	41 087
N_B	37	106	120	1274	283	126	78	41 598
A_{FB}	0.060	−0.057	0.147	−0.004	0.027	−0.237	0.040	0.012
	±0.114	±0.071	±0.059	±0.020	±0.042	±0.069	±0.082	±0.003
Weinberg:				0.241				0.234
$\sin^2\theta_W$				±0.024				±0.002

Table 8: Forward-backward asymmetry of the muon decay channels calculated by investigating the number of events in forward/backward direction. At $E_{CMS} \approx M_Z$ the Weinberg angle can be determined with equation 3.

5.3.3. Lepton universality

In equation 6 it can be seen, that the cross sections of leptons are equal at the Z^0 resonance. To verify that, we have a closer look at the cross sections at $E_{CMS} = 91.22\,\text{GeV}$. From table 7 we get the following results:

$$\sigma_e = (1.85 \pm 0.03)\,\text{pb}$$
$$\sigma_\mu = (1.79 \pm 0.03)\,\text{pb}$$
$$\sigma_\tau = (1.70 \pm 0.03)\,\text{pb}$$

From lepton universality one expects these cross sections to be the same. For the electrons and the muons the deviation is small, nevertheless larger than one standard deviation. The largest deviation can be found for the τ cross section. There could be numerous reasons for the observed deviations.

The τ channel is experimentally difficult to reconstruct due to the different decay channels of the τ itself. Additionally, the center of mass energy of 91.22 GeV is in general not equivalent to the Z^0 mass. Also all considered processes may be subject to statistical fluctuations and systematical errors. For a more thorough explanation of these effects see section 5.3.7.

To inspect the lepton universality further, the ratio of the hadronic to the leptonic channel is calculated in the following:

$$R_e = \frac{\sigma_{had}}{\sigma_e} = 21.97 \pm 0.42$$
$$R_\mu = \frac{\sigma_{had}}{\sigma_\mu} = 22.62 \pm 0.38$$
$$R_\tau = \frac{\sigma_{had}}{\sigma_\tau} = 23.82 \pm 0.45$$

From [9] the expected quantity is $R = 20.771 \pm 0.032$. Again, the τ-value shows the largest deviation and the deviations for the other decay channels are not negligible. Possible effects have been discussed. However it can be concluded, that our results at least are in the right order of magnitude.

5.3.4. Breit-Wigner distribution

The cross sections of the processes can be described by a Breit-Wigner distribution of the following form:

$$\sigma_f = \frac{12\pi}{M_Z^2} \cdot \frac{s\Gamma_e\Gamma_f}{(s - M_Z^2)^2 + s^2\Gamma_Z^2/M_Z^2} \tag{10}$$

Here, Γ describes the decay width of the corresponding particle.
To verify this relation, we plot the cross sections of the different decay channels and fit the equation given above. The diagrams can be seen in figure 14. The resulting fit-parameters $\Gamma_e\Gamma_f$, M_Z and Γ_Z and their errors can be found in table 9.

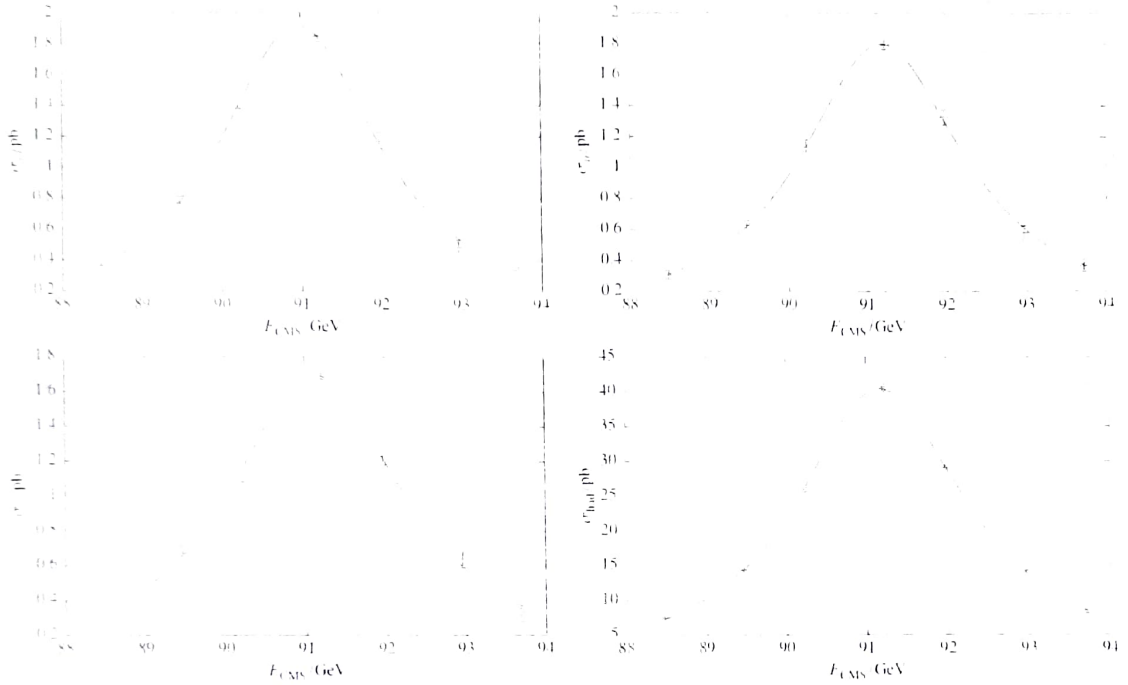

Figure 14: Cross sections of the four decay channels in dependence of the center of mass energy. A Breit-Wigner distribution is fitted (see equation 10).

	$\Gamma_e\Gamma_f \cdot 10^3/\mathrm{GeV}^2$	M_Z/GeV	Γ_Z/GeV	p-value	χ^2_r
e	6.631 89 ± 0.4227	90.983 ± 0.038	2.474 ± 0.095	0.2649	1.31
μ	6.484 96 ± 0.1433	91.203 ± 0.015	2.518 ± 0.032	0.9165	0.24
τ	6.922 89 ± 0.544	91.143 ± 0.053	2.682 ± 0.122	0.0722	2.15
had	152.137 ± 2.879	91.190 ± 0.013	2.572 ± 0.031	0.0329	2.26
mean		91.130 ± 0.059	2.562 ± 0.035		

Table 9: Fit parameters of the Breit-Wigner distribution. To quantify the quality of the fit, the p-value and the reduced chi-squared χ^2_r is given.

Goodness of fit In table 9 two parameters which describe the quality of a fit are listed. The reduced chi squared χ^2_r is the weighted sum of squared deviations per degree of freedom. In our case there are 4 degrees of freedom (number of data points − number of fit-parameters).

In this variable one can assume, that the fit for the electrons is the best (χ^2_r close to 1). In the other channels, there is a larger difference, which means that either the fit is not very good or the uncertainties have been underestimated.
The second variable is the p-value. In this case the electron and muon channel reach values of 25 % and

92 % respectively. The lowest p-value is reached in the hadronic channel. This could be explained by the large number of events in this channel, which leads to smaller uncertainties. It is safe to assume, that the Breit-Wigner distribution is an idealisation of the real decay. Thus smaller errors lead to a deficient convergence of the fit algorithm.

The fit-parameters allow us to specify the mass of the Z-boson and its width. For that the mean of M_Z and Γ_Z of all the channels are given in table 9. The associated literature values are from [9]:

$$M_Z = (91.188 \pm 0.002)\,\text{GeV}$$
$$\Gamma_Z = (2.495 \pm 0.002)\,\text{GeV}$$

The mass lies within one standard deviation of this value, the width lies within two standard deviations.

5.3.5. Partial width of the channels

To determine the width of the channels the parameter $\Gamma_e \Gamma_f$ can be used. Beginning with $\Gamma_e = \sqrt{\Gamma_e \Gamma_e}$ we get the results given in Table 10.

	Γ_{calc}/MeV	Γ_{lit}/MeV/	σ_f^{peak}/pb
e	81.44 ± 2.60	83.91 ± 0.12	1.78 ± 0.32
μ	79.63 ± 3.09	83.99 ± 0.18	1.74 ± 0.36
τ	85.01 ± 7.21	84.08 ± 0.22	1.86 ± 0.25
had	1868.17 ± 69.24	1744.4 ± 2.0	40.84 ± 1.35

Table 10: Partial width of the decay channels, their literature values from [9] and the cross sections determined with equation 11. In general, they agree with the results of section 3.2.

In comparison with the values given in [9] the results are similar. In the case of the hadrons there is a larger deviation of 7 %.
With the values of the width in combination with the other fit-parameters it is also possible to calculate the cross sections in the peak with formula 6 from section 3.2:

$$\sigma_f^{\text{peak}} = \frac{12\pi}{M_Z^2} \frac{\Gamma_e \Gamma_f}{\Gamma_Z^2} \tag{11}$$

The results are listed in table 10 and are comparable to the calculated values of exercise 2 (section3.2) of the preliminary tasks.

5.3.6. Number of generations of light neutrinos

With the done analysis it is now possible to determine the number of neutrino families in the following way: The total decay width of the Z-boson can be written as the sum of the width of all decay channels, as can be seen from equation 1.
This relation is valid if there are only the listed parts and with this formula only contributions of neutrinos under the Z^0-mass are included. The width of the neutrinos is $\Gamma_\nu = (166.33 \pm 0.50)\,\text{MeV}$ (see [9]). In combination with the values of table 10 we obtain:

$$n_\nu = 2.69 \pm 0.47 \tag{12}$$

This value agrees perfectly with $n_\nu = 3$ in one standard deviation. Therefore it can be concluded that there are 3 light neutrino families.

5.3.7. Discussion

Doing the analysis of OPAL data all errors are based on the statistical fluctuation of the event number: $\Delta N = \sqrt{N}$. Nevertheless there are physical processes, which influence the uncertainty of the calculated constants and values systematically.
Systematic uncertainties of the OPAL detector are unknown to us and a complete determination would be beyond the scope of this report. Aspects like the efficiencies of the different detectors and coverage of the solid angle are unknown and thus neglected.

In general the chosen cuts are not perfect. They are based on observations of the histograms, which can lead to errors. Of course, the efficiency matrix should minimize the amount of incorrectly assigned events, but the Monte-Carlo simulated data was only provided for one energy. Additionally, in a simulation one may also need approximations which do not completely represent reality. So also the efficiency matrix can contain systematic uncertainties.

Another point are the radiative corrections. There are no uncertainties or information given about their background. So they are considered to be flawless.